Raman spectroscopy of intercalated and misfit layer nanotubes

Matthias Staiger,[1,*] Vladimir Bačić,[2] Roland Gillen,[1] Gal Radovsky,[3] Konstantin Gartsman,[4] Reshef Tenne,[3] Thomas Heine,[2,5] Janina Maultzsch,[1] and Christian Thomsen[1]

[1]*Institut für Festkörperphysik, Technische Universität Berlin, Hardenbergstr. 36, 10623 Berlin, Germany*

[2]*Department of Physics and Earth Sciences, Jacobs University Bremen gGmbH Campus Ring 1, 28759 Bremen, Germany*

[3]*Department of Materials and Interfaces, Weizmann Institute of Science, Rehovot 76100, Israel*

[4]*Electron Microscopy Unit, Weizmann Institute of Science, Rehovot 76100, Israel*

[5]*Wilhelm-Ostwald-Institut für Physikalische und Theoretische Chemie, Linnéstr. 2, 04103 Leipzig, Germany*

(Received 12 January 2016; revised manuscript received 23 June 2016; published 18 July 2016)

We present Raman spectra of misfit layer $(PbS)_{1.14}NbS_2$ nanotubes and lead intercalated NbS_2 nanotubes. They represent interesting model systems to investigate the nature of interlayer interaction in layered materials. A direct correlation to the Raman modes of the parent $2H$-NbS_2 compound exists, but some modes are seen drastically upshifted in frequency in the misfit layer and intercalated compound while others remain almost unchanged. On the basis of the Raman spectroscopic investigations and with the help of supporting calculations we examine different interlayer bonding mechanisms and contribute to the discussion as to why these frequency shifts occur.

DOI: 10.1103/PhysRevB.94.035430

I. INTRODUCTION

In recent years transition metal dichalcogenide nanostructures (TMDCs) attracted a lot of interest. TMDCs span a wide variety of structures and physical properties, ranging from isolators to semiconductors, metals, and superconductors. Like for carbon based compounds, dimensionality is an important factor determining the properties of TMDCs. Apart from mono- and few-layer quasi-two-dimensional structures a number of TMDC nanotubes has been successfully synthesized [1]. Recently, there were first reports on the synthesis and characterization of nanotubes consisting of alternating layers of SnS/PbS and SnS_2/NbS_2 rolled up so as to reduce the lattice mismatch between the two materials [2–4]. These nanotubes belong to the family of misfit layer compounds (MLCs) composed of transition metal dichalcogenides TX_2 (T = Ti, V, Cr, Nb, Ta and the main group metal Sn; X = S, Se) and layers MX and RX (M = Sn, Pb, Sb, Bi, R = rare earth metals).

In their bulk form MLCs have been investigated for decades [5–8], and research has made evident that the possibility of combining these very different classes of materials makes for a plethora of structures and physical properties. They all have in common that they crystallize in highly ordered anisotropic structures, as will be detailed below. Consequently, research has always been accompanied by the question as to why these structures are so remarkably stable. A diverse set of methods ranging from (angle-resolved) photoelectron spectroscopy [9,10], electron microprobe analysis [11], photoemission microspectroscopy [12], bond valence [13] and *ab initio* density functional calculations [14], and not least Raman spectroscopy [15–19] have all been dedicated to gain insight into the nature of interlayer interaction governing the overall stability of MLCs. Apart from the intrinsic importance of MLCs as a model system for studying interlayer interaction and how intercalation can change the electronic properties of the host structure in layered systems, MLCs exhibit interesting thermoelectric properties [20–23], and many of them are superconductors [24]. With current research on layered materials increasingly focusing on low-dimensional systems, an ever growing family of tubular misfit layer compounds has been recently synthesized [2–4,25–27], but studies on their electronic and optical properties are as yet scarce [28]. In this context the present study aims to revisit studies on the properties of bulk MLCs and apply the findings to their nanostructured counterparts. Here, Raman spectroscopy has been the method of choice as it not only uncovers the vibrational properties but provides information about the electronic structure of the investigated materials. As such, this study contributes to the deciphering of the nature of interlayer interaction in tubular misfit layer nanostructures. The focus lies on representatives of a larger family of nanotubes, $(PbS)_{1.14}$-NbS_2 and Pb-intercalated NbS_2 nanotubes, where both components are low temperature superconductors [29].

Structurally similar to their bulk counterparts, in the rolled up TX_2 layers, transition metal atoms are sandwiched between six chalcogenide atoms whereas the MX and RX layers commonly adopt a distorted rock salt structure. The layers are stacked along the c axis. With a few exceptions, the layers share a common b axis length. The a axes are incommensurate meaning that the ratio of the two a sublattice constants is irrational. This affects the stoichiometry of the overall system which is expressed by the index x in $(MX)_xTX_2$.

In $(PbS)_{1.14}NbS_2$, a two atoms thick part of the PbS bulk structure is cut out to form a planar composite structure alternating with NbS_2 layers. The cubic symmetry of the lead sulfide layer is broken in the misfit layer compound with the Pb atoms protruding into the van der Waals gap between the layered subsystems. Electronically, bulk PbS is a narrow-gap semiconductor (E_{gap} = 0.42 eV [30]). NbS_2 crystallizes in trigonal prismatic coordination, where the Nb atom is placed between six sulfur atoms forming two tetrahedrons. In contrast to other $2H$-dichalcogenides like MoS_2 and WS_2, which exhibit a transition from an indirect to a direct band gap material once the thickness has been reduced to

*Corresponding author: mstaiger@physik.tu-berlin.de

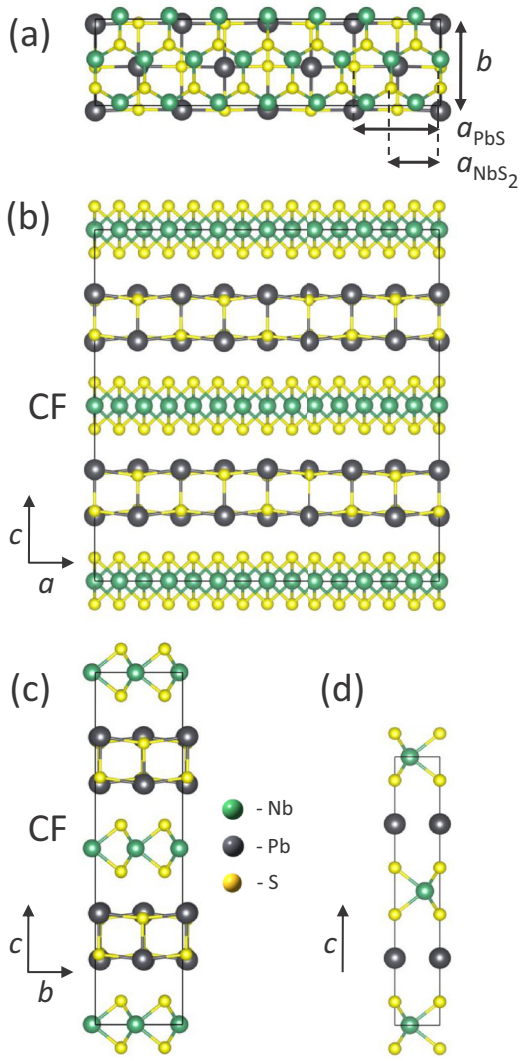

FIG. 1. (a) Structure of the misfit layer compound $(PbS)_{1.14}NbS_2$ in the a-b plane. The ratio of the a axes is irrational, therefore the compounds are classified as misfit layer compounds (MLC). (b) and (c): The structure of the misfit compound viewed along the commensurate b and the incommensurate a direction, respectively. (d) View along the normal to the (11.0) plane according to the pseudo-hexagonal system of labeling of the NbS_2 material intercalated with lead atoms in linear coordination to neighboring S atoms (ICSD col. code. 74698).

a monolayer, NbS_2 stays a metal even in the two-dimensional limit [31]. The metal character stems from a partially filled $4d_{z^2}$ Nb orbital around the Fermi energy. In the misfit layer compound (MLC) the NbS_2 layers remain fairly rigid and almost preserve the structure of the pristine $2H$-NbS_2 [14]. Figure 1(a) shows a view on the a-b plane of the $(PbS)_{1.14}NbS_2$ compound. In the simple orthorhombic conventional unit cell, the sublattices share a common b lattice constant, but the a lattice constants stay incommensurate with a lattice ratio of $a_{PbS}/a_{NbS_2} \approx \sqrt{3}$ which makes for $4a_{PbS} \approx 7a_{NbS_2}$ [32]. In Figs. 1(b) and 1(c) a view along the two in-plane lattice directions is depicted. Along the c direction, the CF stacking sequence is common in bulk $(PbS)_{1.14}NbS_2$ [7], but loses its validity in the misfit nanotubes. The conventional unit cell contains 28 units of NbS_2 and 32 units of PbS, which makes for the index of 1.14. Between the layers, besides the van der Waals interaction, some coordinative bonding may exist. In misfit layer compounds, the MX material is often characterized as the intercalant in between the TX_2 layers.

This is also the case in the second type of nanotubes investigated in this study, Pb-NbS_2 nanotubes, where the lead undoubtedly can be described as an intercalant. Here, the Pb atoms are, rather unusually, linearly coordinated to two S atoms of the adjacent NbS_2 slabs, as can be seen in Fig. 1(d). Thus in the c direction not the metal atoms but the S atoms are found on top of each other [4,33]. The expected atomic ratio of 1:1 between the niobium and the lead atoms was confirmed previously in Ref. [34]. Strictly speaking, the Pb-NbS_2 nanotubes are thus not misfit layer compounds but, as we will see, the intercalants have strikingly similar effect on the Raman spectra of the host NbS_2 layer as the lead sulfide layers in the MLC.

In this paper we present Raman spectra of $(PbS)_{1.14}NbS_2$ nanotubes and NbS_2 nanotubes intercalated with lead. While the vibrational properties of the former can be compared to its parent material, the latter has not been investigated before. Our focus lies on the changes in the Raman frequencies of the misfit layer and intercalated materials compared to the pristine compound. The different mechanisms of interlayer bonding are critically discussed on the basis of the results of the Raman spectroscopic investigation. The popular charge transfer hypothesis is challenged experimentally as well as theoretically, and we propose an alternative way to explain the drastic Raman frequency upshifts observed in both compounds.

A. Experiment

Pb-Nb-S tubular structures were synthesized via chemical vapor transport technique in evacuated quartz ampules as was described in Ref. [4]. Reference [4] also describes in detail the characterization process. Prior to Raman measurements (high resolution) TEM images were taken of each nanotube and the respective type was identified by determining the layer periodicities. In Fig. 2(a) this can be seen for a Pb-NbS_2 nanotube with 0.88 nm periodicity (NbS_2 layer and atomic Pb layers are alternating). The same is shown for a $(PbS)_{1.14}NbS_2$ misfit layer nanotube in Fig. 2(b). Here, PbS and NbS_2 layers are alternating, resulting in a 1.20 nm periodicity. Additionally, energy-dispersive x-ray (EDS) spectra and selected area electron diffraction (SAED) patterns were at hand and are described in Ref. [4]. Raman spectra of individual misfit layer nanotubes were recorded in backscattering geometry employing a frequency doubled Nd:YAG laser emitting at 532 nm. The scattered light was analyzed using a LabRam HR spectrometer with a 600/mm grating and a Peltier-cooled charge-coupled device. The spectral resolution was approximately 2 cm^{-1}. Laser power had to be limited to 130 μW so as to avoid burning the underlying thin carbon TEM substrate. Due to the investigated materials being rather poor Raman scatterers, accumulation times exceeded 20 minutes in most cases and several spectra recorded at the same position of the sample had to be summed to get appreciable signal.

Density functional theory (DFT) calculations were carried out using the local-density approximation (LDA), with

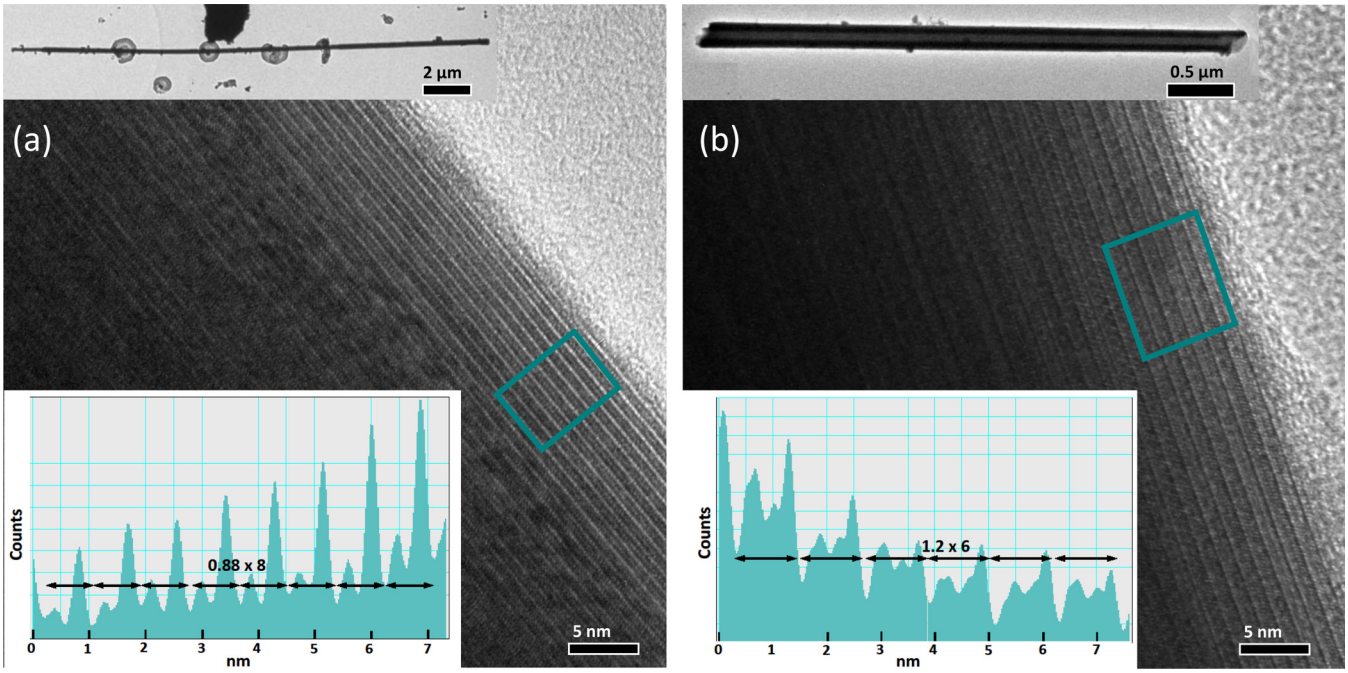

FIG. 2. Structural characterization of the nanotubes. (a) High and low (inset) TEM images of a Pb-NbS_2 nanotube investigated in this paper. The layer periodicity of 0.88 nm (alternating layers of Pb atoms and NbS_2) can be identified in a line profile (inset) of the nanotube area enclosed by the rectangle. (b) High and low (inset) TEM images of a $(PbS)_{1.14}NbS_2$ misfit layer nanotube investigated in this paper. The line profile (inset) taken from the area enclosed by the rectangle depicts the layer periodicity of 1.20 nm corresponding to alternating layers of PbS and NbS_2.

plane-wave basis and the projector-augmented wave (PAW) method, as implemented in the Quantum ESPRESSO (QE) package [35]. The Brillouin zone (BZ) was sampled using a $24 \times 24 \times 6$ Monkhorst-pack (MP) grid for NbS_2 and Pb-NbS_2, and a $3 \times 12 \times 3$ MP grid for $(PbS)_{1.14}NbS_2$. The cutoffs for plane-wave and charge-density expansion were set to 65 Ry and 650 Ry, respectively. Threshold for structural optimization was set to 2 (meV/Å)/atom in all three structures. Phonon frequencies were calculated using the linear-response (DFPT) technique, again within the QE package. To obtain the entire phonon dispersion in the case of NbS_2 and Pb-NbS_2, dynamical matrices were calculated on a $6 \times 6 \times 1$ MP grid in the BZ. Although the measurements were done on nanotubes, in the calculations a three-dimensional system, with the unit cells given in Fig. 1, was assumed. Since the studied nanotubes are $\gg$100 nm in diameter and the number of walls are well above ten in all cases studied, this is assumed to be a good approximation.

B. Results

Raman spectra of $2H$-NbS_2 were obtained by Nakashima *et al.* [36] thirty years ago. The two main Raman modes were observed at 379 cm^{-1} (A_{1g}) and 309 cm^{-1} (E^1_{2g}). In the regular $(PbS)_{1.14}NbS_2$ nanotubes, PbS and NbS_2 walls are alternating [4]. Coming from the bulk $2H$-NbS_2 D^4_{6h} structure, the symmetry of the NbS_2 part is at least reduced to the monolayer D_{3h} structure; additional distortion might occur due to charge transfer, covalent interlayer bonding, and nanotube curvature. However, in this paper, Raman mode assignments are based on the D_{3h} structure for simplicity. Due to the lack of a center of inversion, the bulk A_{1g} and B_{1u} modes reduce to A'_1 symmetry, and the E^1_{2g} and E_{1u} modes become in-plane E' modes. In backscattering geometry, the E'' mode (E_{1g} and E_{2u} in the bulk) is Raman forbidden. In total, the irreducible representations of the phonon modes in the symmetry group D_{3h} at the Γ point of the hexagonal Brillouin zone are $\Gamma = A'_1 + E'' + 2A''_2 + 2E'$.

From the bulk PbS structure, a two atoms thick part is cut out to form the PbS walls. They are significantly distorted compared to the NaCl type parent material with the lead atoms always protruding into the van der Waals gap. In contrast to the three-dimensional bonding network of bulk PbS, first-order Raman scattering becomes allowed [15].

Figure 3(a) shows Raman spectra of $(PbS)_{1.14}NbS_2$ nanotubes. Two regions can be singled out: below 200 cm^{-1} with Raman modes that have been attributed to the PbS layers in the literature [15,18,37] and above 340 cm^{-1}, where the two main peaks can be identified as the E' and A'_1 mode of the NbS_2 layer [15,38]. The A'_1 mode is situated at $\sim$378 cm^{-1} and thus only very weakly downshifted with respect to the A_{1g} mode of bulk NbS_2. A drastic change in Raman frequency on the other hand is observed for the E' mode that is upshifted by more than 40 wave numbers compared to the E_{2g} mode of bulk NbS_2 and lies at $\sim$353 cm^{-1}. The upshift is up to 12 wave numbers stronger than that found in bulk $(PbS)_{1.14}NbS_2$ [15,18,37,38]. Possible reasons for this rather unusual behavior, such as charge transfer from the MX to the TX_2 layer, strain effects, interlayer bonding, and the monolayer nature of the TX_2 part, will be discussed in detail in the next section. Typical full widths at half maximum (FWHMs) of the E' and A'_1 mode are 13 cm^{-1} and 15 cm^{-1}, respectively. Surprisingly, the relative intensities of the two

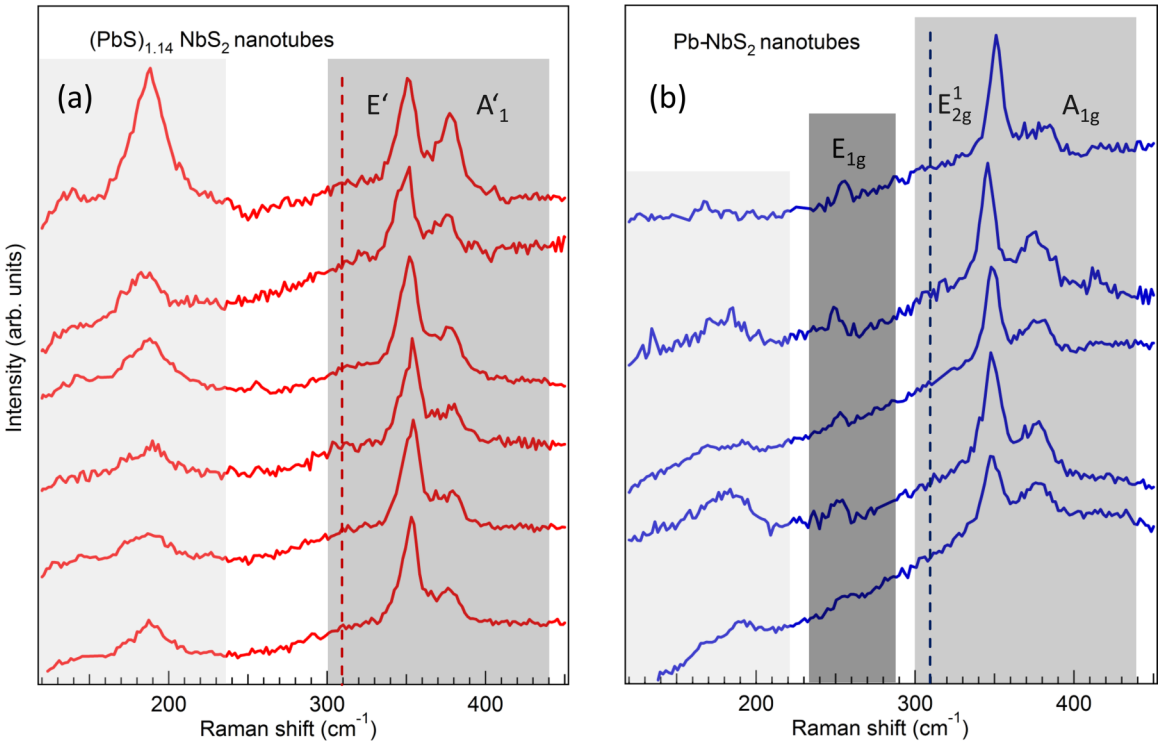

FIG. 3. (a) Raman spectra of all measured $(PbS)_{1.14}NbS_2$ nanotubes. The spectra of the different nanotubes have in common that they can be divided into two regions with modes associated with the PbS part below 200 cm^{-1} (light gray) and the main E' and A_1' Raman modes of the NbS_2 part between 300 and 400 cm^{-1} (darker gray). (b) Raman spectra of all measured Pb-NbS_2 nanotubes. Again, modes probably associated with the intercalant are found below 200 cm^{-1} and NbS_2 E_{2g}^1 and A_{1g} modes above 300 cm^{-1}. A Raman feature not seen in $(PbS)_{1.14}NbS_2$ nanotubes is the mode around 250 cm^{-1} (darkest gray). It is likely to be the E_{1g} mode of the NbS_2 part. Spectra depicted in (a) and (b) are taken with 532 nm excitation wavelength. They are normalized to the E mode around 350 cm^{-1} and offset for clarity. The solid lines represent the position of the E_{2g}^1 mode in the pristine $2H$-NbS_2 material (309 cm^{-1}) [36].

modes are different from the ones previously observed for the bulk MLC. For the nanotubes investigated in this paper the intensity ratio E'/A_1' has values close to 2.5, whereas for the bulk structures the ratio is almost reversed [15]. However, in the literature, the Raman spectra are recorded with 488 nm or 514 nm excitation wavelength [15,37] in contrast to the 532 nm laser light used here. In both the parent $2H$-NbS_2 material and the bulk $(PbS)_{1.14}NbS_2$ compound, strong two-phonon bands are identified [15,36] that are apparently absent in the misfit layer nanotubes. Between 100 and 200 cm^{-1} three modes can be distinguished in most of the Raman spectra (see Fig. 3); a rather strong peak at 187 cm^{-1} with a shoulder at 170 cm^{-1} and a weak broad feature around 140 cm^{-1}. The latter is close to the cutoff of the notch filter and thus possibly reduced in intensity.

The Raman spectra of Pb-NbS_2 nanotubes are shown in Fig. 3(b). They can be easily related to the spectra of $(PbS)_{1.14}NbS_2$ nanotubes described above. There are, however, subtle differences between the two cases. Even though the original structure of the $2H$-NbS_2 parent material is changed both by the intercalated Pb atoms and the resulting stacking arrangement, the high D_{6h}^4 symmetry is retained. The vibrational modes of the material as a whole can thus be decomposed into the following irreducible representations at the Γ point of the Brillouin zone: $\Gamma = A_{1g} + 2A_{2u} + 2B_{2g} + B_{1u} + E_{1g} + 2E_{1u} + 2E_{2g} + E_{2u}$.

Two of the four Raman active modes can be easily identified in the measured Raman spectra. The A_{1g} mode is broadened compared to the closely related A_1' mode in $(PbS)_{1.14}NbS_2$ ($\sim$378 cm^{-1}) and slightly downshifted to $\sim$377 cm^{-1}; the E_{2g}^1 mode is always located at lower Raman frequencies than the corresponding E' mode in the $(PbS)_{1.14}NbS_2$ nanotubes ($\sim$353 cm^{-1}), namely at $\sim$348 cm^{-1}. The relative intensities are $E_{2g}^1/A_{1g} = 1.5$ in average. In the lower-wave-number region, weak Raman features appear at almost the same frequency as in the misfit compound, namely at $\sim$187 and 169 cm^{-1}. In comparison with the Raman spectra of $(PbS)_{1.14}NbS_2$, the peak at 169 cm^{-1}, which is only seen as a shoulder of a stronger peak in $(PbS)_{1.14}NbS_2$, is of higher relative intensity in Pb-NbS_2. Most importantly, a feature that allows for the easy identification of NbS_2 nanotubes with intercalated lead atoms is the appearance of a new Raman feature at around 253 cm^{-1} that is not observed in the spectra of the $(PbS)_{1.14}NbS_2$ nanotubes.

II. DISCUSSION

A. Raman modes between 100 and 200 cm^{-1}

It is commonly accepted in the literature on misfit layer compounds that the Raman spectra can be divided into a higher-frequency part with Raman modes belonging to the host material and a lower-lying part with Raman modes of the intercalant. Whereas the NbS_2 modes in the Raman spectra of $(PbS)_{1.14}NbS_2$ and Pb-NbS_2 can be easily identified by

comparison with the bulk parent material, this cannot be said about the MX part of the structure. First-order Raman scattering is not allowed for the original three-dimensional bulk PbS structure but becomes possible in the distorted double-layer structure of PbS in $(PbS)_{1.14}NbS_2$. In principle, three sources for the Raman features between 100 and 200 cm^{-1} are conceivable in the MLC: (i) phonons stemming from the PbS part of the MLC, (ii) second-order modes and two-phonon density of states, or (iii) defect, disorder-induced modes.

(i) The main peak at 189 cm^{-1} in the Raman spectra of the MLC nanotubes is observed in the Raman spectra of the bulk MLC as well [15,18,37] and has been identified as one of two PbS modes of A type symmetry. By comparison with a work by Kisoda *et al.* [17] on misfit layer compounds of $2H$-TaS_2 it is likely to be the symmetric layer breathing mode of PbS; the frequency of the other A type mode of PbS was reported to be around 80 cm^{-1} [15], too low-lying to be observed in this paper. As a rather surprising result, the mode at 189 cm^{-1} that could be related to PbS still occurs in the spectra of Pb-NbS_2 nanotubes (albeit with only weak Raman intensity), despite the assumption that no lead sulfide layers are present in the structure. This raises the question whether there are "pockets" of PbS still present in the structure of the Pb-NbS_2 nanotubes that result in PbS modes depending on the local environment. This would also explain the different intensities observed for different Pb-NbS_2 nanotubes. Another idea would be that a nearly covalent bonding of Pb atoms to the neighboring NbS_2 layers could give rise to a PbS-like phonon density of states.

(ii) The peak at 189 cm^{-1} is rather broad, which is unusual for a first order Raman mode but typical for a two-phonon band. Very broad two-phonon bands appear in the spectra of bulk $2H$-NbS_2 at higher wave numbers between 200–300 cm^{-1} [36] and are unlikely to be accountable for the features just below 200 cm^{-1} in the MLC. It seems possible that second order modes of the intercalant appear in the spectra of the MLC as well as in Pb-NbS_2. The phonon dispersion of Pb-NbS_2 is shown in Fig. 4(b); for comparison the phonon dispersion of the parent $2H$-NbS_2 is depicted in Fig. 4(a). At the Γ point one can see the two first order Pb-NbS_2 modes at 364 and 388 cm^{-1}, but there are also lower-lying modes at 66, 98, and 103 cm^{-1}. The atomic displacement patterns (not shown) reveal for the second of these modes that the Pb atoms and NbS_2 vibrate against each other as rigid layers; for the third mode NbS_2 layers perform breathinglike motions while the Pb layer is not vibrating. Second-order scattering of both of these modes could in principle be responsible for the Raman features seen at 189 and 170 cm^{-1} in Pb-NbS_2. The question then arises if similar patterns would be observable in the misfit layer compound with the PbS layer playing the role of the intercalant atoms in Pb-NbS_2.

(iii) Raman spectra of the $3R$-NbS_2 polytype exhibit a broad phonon band centered around 160 cm^{-1} [36,39]. McMullan *et al.* [39] attribute it to an impurity or defect mode possibly resulting from the expected nonstoichiometry of $3R$-NbS_2 with some extra Nb atoms located in the van der Waals gap [40]. One might argue that the situation here is similar. Both $3R$-NbS_2 and Pb-NbS_2 as well as the misfit layer compound have different stacking orders compared to $2H$-NbS_2, and all three of the compounds exhibit a strong upshift of the E^1_{2g} mode compared to $2H$-NbS_2. As we will discuss later, there is strong likelihood of metal cross substitution in the misfit layer compound [12]. The exchange of Pb atoms in the PbS layer with Nb atoms of the NbS_2 layer and vice versa could indeed lead to an impurity-induced Raman mode in the spectra of the $(PbS)_{1.14}NbS_2$ nanotubes. The feature at around 140 cm^{-1}

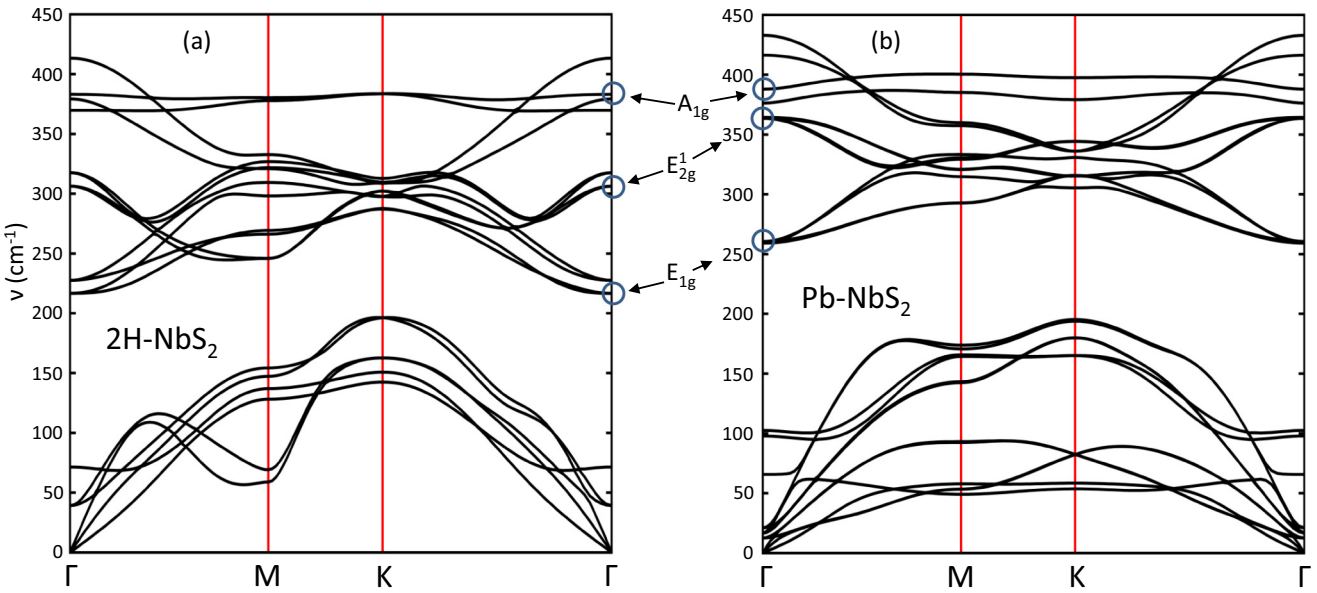

FIG. 4. (a) Phonon dispersion of the parent $2H$-NbS_2 bulk material. Above 200 cm^{-1} at the Γ point, three first order Raman modes, the E_{1g}, E^1_{2g}, and A_{1g} mode, are marked with blue circles and their calculated frequencies are listed in Table I. (b) The main features of the dispersion are reproduced in the dispersion of lead intercalated NbS_2. The three main Γ-point Raman modes are seen above 250 cm^{-1}, with the two E type modes considerably upshifted compared to their frequency in NbS_2. The frequency of the A_{1g} mode, on the other hand, stays nearly the same. Modes with contributions from the intercalant lead atoms are found around 100 cm^{-1}.

in the $(PbS)_{1.14}NbS_2$ nanotubes has not been conclusively attributed in the literature [37]. A feature observed at 165 cm^{-1} in the misfit layer compound $(LaS)_{1.2}NbS_2$ [16] is ascribed to a mode induced by the interaction of the two components; that is, the modulation along the *a* axis in the LaS layer. The fact that the 140 cm^{-1} mode has no significant intensity in Pb-NbS_2 indeed is evidence of this mode being a Raman mode inherent to the misfit compound.

B. Raman modes belonging to NbS_2 in the $(PbS)_{1.14}NbS_2$ and Pb-NbS_2 nanotubes

Both NbS_2 and PbS Raman modes are observed in the spectra of the misfit layer nanotubes. In particular, the character of the two prominent NbS_2 modes is preserved as has been shown by polarization dependent Raman measurements on bulk $(PbS)_{1.14}NbS_2$ and other similar compounds [16,37]. Hence, the Raman spectra can be considered as a superposition of contributions from their constituents. In the investigated wave-number region, no new Raman modes were observed that would point to structural changes or significant electronic interaction between the layers of the two materials. Neither did we observe Raman bands that could be assigned to Raman inactive modes or phonons in violation of the $q = 0$ selection rule. Despite this apparent independence of the alternation of layers, some modes are found to be considerably shifted in frequency from those of the pristine crystals. Most prominently, the E'/E^1_{2g} mode of the NbS_2 material is upshifted by more than 40 wave numbers to 353 and 348 cm^{-1} in $(PbS)_{1.14}NbS_2$ and Pb-NbS_2 nanotubes, respectively. Possible strain effects would be expected to be much smaller. The cell parameter of the NbS_2 part in the commensurate *b* direction is slightly increased in the MLC with respect to 2*H*-NbS_2 to match the cell parameter of the PbS part [32]. In fact, a softening of Raman frequencies from the resulting tensile strain would be expected, opposite to what is observed here.

In Fig. 5(a) the region of the in-plane *E* mode and the out-of-plane *A* mode is shown for exemplary nanotubes of both types. Again, the A'_1/A_{1g} mode is rather broad and has similar frequency in the two compounds, whereas the E'/E^1_{2g} is of smaller FWHM especially in the Pb-NbS_2 nanotubes. While the *E* mode is shifted drastically with respect to the 2*H*-NbS_2 parent compound (309 cm^{-1}), the shift is a few wave numbers smaller in Pb-NbS_2 than in $(PbS)_{1.14}NbS_2$. Although there is some spreading in the absolute frequencies of the *E* and *A* modes, the frequency difference between the two modes is always bigger in Pb-NbS_2 than in $(PbS)_{1.14}NbS_2$, as is shown in Fig. 5(b). Hence the two types of nanotubes investigated in this study can be easily distinguished. We have calculated the frequencies of the first order Raman modes of bulk 2*H*-NbS_2, Pb-NbS_2, and $(PbS)_{1.14}NbS_2$ as detailed in the experiment section and present them in Table I. The calculated frequencies of 2*H*-NbS_2 are in excellent agreement with the experimentally obtained frequencies taken from Ref. [36]. The calculated E_{1g} NbS_2 mode is not reported in Ref. [36] because it is forbidden in the employed backscattering configuration. Employing the same method to the Pb-NbS_2 and $(PbS)_{1.14}NbS_2$ bulk compounds, we find a good agreement between measured and calculated frequencies. The calculations confirm the strong upshift of the E^1_{2g}/E' in Pb-NbS_2 and $(PbS)_{1.14}NbS_2$ as compared to the 2*H*-NbS_2 parent material and the only small changes in the A_{1g}/A'_1 frequency. The calculations on the misfit compound reveal a splitting of the mentioned modes into several components which could account for the experimentally observed broadening of the modes with respect to the parent material. For the misfit compound we can also see that the calculations are in excellent agreement with bulk literature values. However, even though

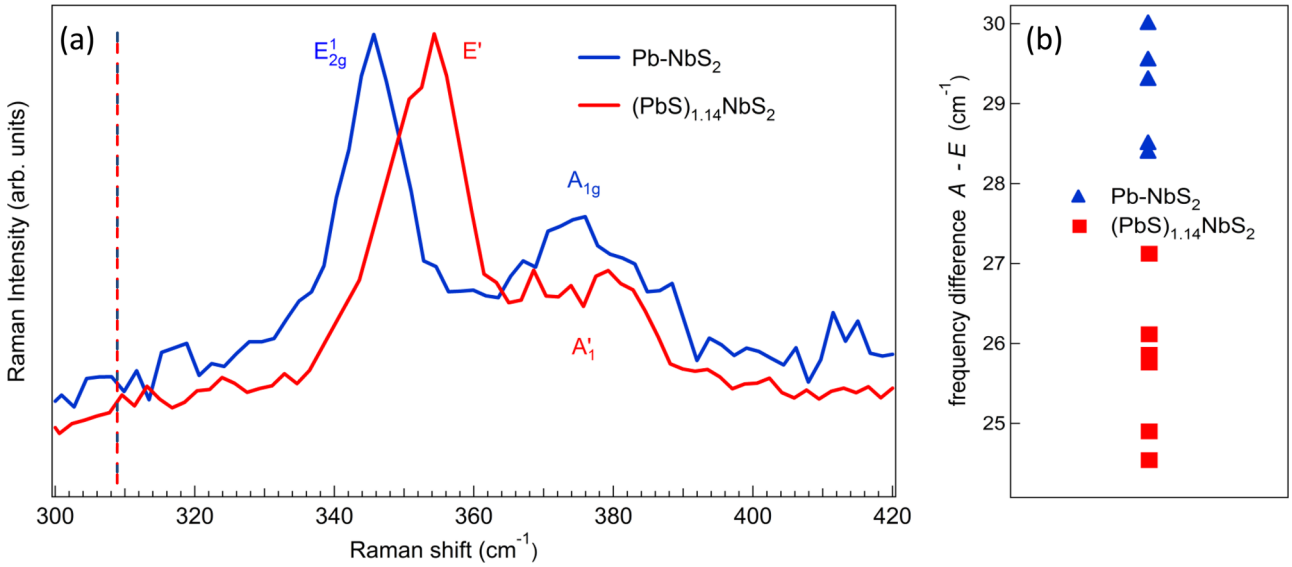

FIG. 5. (a) Raman features in the region between 300 and 420 cm^{-1} of exemplary Pb-NbS_2 and $(PbS)_{1.14}NbS_2$ nanotubes. The most prominent intralayer NbS_2 modes in the investigated compounds are shown with the in-plane E' of $(PbS)_{1.14}NbS_2$ (red line) always at slightly higher frequencies than the E^1_{2g} mode of Pb-NbS_2 (blue line). Again, the dashed line represents the position of the E^1_{2g} mode in the pristine 2*H*-NbS_2 material (see Fig. 3) [36]. In contrast, the A'_1 mode of $(PbS)_{1.14}NbS_2$ is found at nearly the same frequency as the A_{1g} mode in Pb-NbS_2. (b) The frequency difference between the above described modes clearly distinguishes the two types of nanotubes, with $\omega(A\text{-}E)$ between 24–27 cm^{-1} for all of the measured $(PbS)_{1.14}NbS_2$ nanotubes and 28–30 cm^{-1} for all of the Pb-NbS_2 nanotubes.

TABLE I. Calculated and experimentally obtained Raman frequencies (in cm^{-1}) of the bulk $2H$-NbS_2 structure, the lead intercalated NbS_2 material, and the misfit layer $(PbS)_{1.14}NbS_2$ compound. Where available, literature bulk values are added. The in-plane E modes shift up in frequency from the parent material to Pb-NbS_2 and $(PbS)_{1.14}NbS_2$, whereas the out-of-plane A mode remains almost constant.

D^4_{6h} symm.	2H-NbS_2 bulk calc.	2H-NbS_2 bulk exp. [36]	Pb-NbS_2 bulk calc.	Pb-NbS_2 NT exp.	D_{3h} symm.	$(PbS)_{1.14}NbS_2$ bulk calc.	$(PbS)_{1.14}NbS_2$ bulk exp. [37]	$(PbS)_{1.14}NbS_2$ NT exp.
E_{1g}	217		260	253	E''	237, 241		
E^1_{2g}	306	309	364	348	E'	333-340	342	353
A_{1g}	383	380	388	377	A'_1	372-379	375	378

the nanotubes investigated in this paper are hundreds of nanometers in diameter, have a large number of walls, and thus can be considered as bulklike, the measured Raman frequencies in the nanotube deviate somewhat from the bulk values. This is even more so for the intercalated Pb-NbS_2 nanotubes. There is no literature on the Raman spectrum of the Pb-NbS_2 bulk, but bulk calculations and measured nanotube frequencies differ more strongly than in the calculated and measured MLCs. The calculations also show that the E^1_{2g}/E' mode is not the only mode exhibiting an upshift but that similar frequency shifts can be expected for the E_{1g} mode of $2H$-NbS_2 in the intercalated and the misfit compounds. This is in disagreement with Ref. [39], where the authors identify a Raman feature in $2H$-NbS_2 around 260 cm^{-1} as the E_{1g} mode, although they describe their assignment as somewhat tentative as it deviates strongly from their calculated $2H$-NbS_2 phonon frequencies. On the other hand, the Raman mode observed at 258 cm^{-1} in the stage-2 MLC $(LaS)_{0.6}NbS_2$ [16] perfectly fits the picture presented here, as it is also likely to stem from an upshifted $2H$-NbS_2 E_{1g} phonon mode.

Most of the works dealing with Raman spectroscopy on intercalated transition metal dichalcogenides or misfit layer compounds commonly agree that the drastic frequency shifts originate from charge transfer (CT) from the intercalated layer to the TX_2 layer [15,17,18,37]. The MX layer acts as the donor part of the structure, donating electrons to the half-filled d_{z^2} conduction band orbital (one electron per T atom) of the trigonal prismatic TX_2 layer (T = Nb, Ta). Apart from the band filling and resulting shift of the Fermi level to higher energies, following the rigid band model, the electronic band structure closely resembles the superposition of the band structure of the constituent materials. However, no final conclusion has been reached as to why only certain Raman modes are affected strongly by the CT whereas other Raman modes are barely influenced. Pereira *et al.* [41] note that the lobes of the d_{z^2} orbital are oriented in the z direction, perpendicular to the layers. As the atomic displacement vectors for the E-type phonons are in the layer plane, there will be changes in the overlap of the sulfur valence orbitals with the d_{z^2} orbital of the T atom. Therefore, the CT will have a bigger influence on the Raman frequency than for the A'_1 mode, where sulfur atoms from the TX_2 layer move along z. Another way to investigate the consequences of the band filling by the charge transfer is to look at the changes of the intralayer central and noncentral forces. While the former are increased as a result of the CT, the latter angle bending force constants are decreased, affecting the E-type modes in particular [42]. Looking at the magnitude of the charge transfer one has to differentiate between compounds where the TX_2 layer is not stable in itself and only exists in MLCs because it is stabilized by the charge transfer (for instance LaS-CrS_2 [25]), compounds with a stable TX_2 layer and R = La, Ce, Gd (rare earth metals, which are often trivalent in the RX layer of the MLCs) and compounds with a stable TX_2 layer and M = Sn, Pb (post-transition metals that take a divalent state in MX). In the first two cases, a charge transfer mechanism seems well established both experimentally and theoretically, and its magnitude is of considerable strength with up to 0.9 electrons being donated to the d_{z^2} orbital [43–46]. In the case we are dealing with here, however, the charge transfer appears to be weaker. Using a variety of experimental and theoretical methods, a charge transfer of up to 0.4 electrons/Nb atom is reported by a number of authors [18,47,48], while others find no evidence or are in doubt whether there is charge transfer at all [49,50]. This is in agreement with our calculations, which show no sign of charge transfer but, as detailed above, yield Raman frequencies in excellent agreement with literature values. Nonetheless, assuming that charge transfer is responsible for the strong upshift of the E' mode in $(PbS)_{1.14}NbS_2$, the magnitude of this shift should be in some way related to the amount of charge transfer. Indeed, Hangyo *et al.* [38] find that the upshift is stronger by some 20 cm^{-1} for RS-NbS_2 (R = La, Ce) than for MS-NbS_2 (M = Sn, Pb). Furthermore, they substantiate their argument by looking at the Raman spectra of stage-1 and stage-2 compounds, where the MX layer is inserted every TX_2 layer and every second TX_2 layer, respectively. The weaker frequency shift in the stage-2 compounds is attributed to only half the charge being transferred to the NbS_2 layer in the stage-2 compounds as there are only half as many MX layers [37]. Following this picture, the charge transfer should be expected to be of similar strength for both the investigated materials in the present work or even a little weaker for Pb-NbS_2 than for $(PbS)_{1.14}NbS_2$, as evidenced by the slightly smaller frequency shift in the Raman spectra of the former compound. However, Eppinga *et al.* [51] as well as Dijkstra *et al.* [52] made a convincing case that the transferred charge for compounds, where post-transition metal atoms are intercalated between dichalcogenide layers (such as in Pb-NbS_2), is one electron per post-transition metal atom. The NbS_2 d_{z^2} band is then completely filled, and one can instead expect metallic conduction of the remaining electrons in the intercalated layer. Photoelectron spectra of the valence bands as well as the Nb ($3d$) core levels exhibit shifts and increased band filling with respect to the host material spectra, which clearly indicates that charge transfer takes place. The transfer of one electron per Pb atom leads to an "unusual

(formal) valency" of Pb^{+}, but there is evidence that a rapid valency fluctuation between Pb^{0} and Pb^{2+} can account for this average valency [53]. Our QE calculations on the other hand, similarly to the calculations on the misfit compound, show little to no charge transfer from the intercalated atoms to the transition metal dichalcogenide layer.

In summary, the charge transfer process is very important for misfit compounds with rare earth metal chalcogenide layers RX, and there is experimental evidence that it is important for Pb-NbS_2 as well, although this is not supported by our calculations. The same, however, can not be said about $(PbS)_{1.14}NbS_2$ and other MX-TX_2 misfit compounds, where experimental and theoretical evidence points to little to no charge transfer at all. This means that charge transfer alone can not sufficiently explain the strong upshift of the E modes in misfit layer compounds. For $(PbS)_{1.14}NbS_2$ and Pb-NbS_2 more specifically, the amount of suspected charge transfer does not correlate with the magnitude of the Raman frequency upshifts, furthermore rendering improbable the charge transfer mechanism as a way to explain the observed shifts.

Nonetheless, it is the change of interlayer interaction from the pristine to the misfit layer compounds that is not only the key to an understanding of the remarkable stability of MLCs [12] but will also define their vibrational properties. Some of these interlayer interaction mechanisms shall be discussed here.

(i) Among the different possible bonding mechanisms between neighboring MLC layers, Kalläne *et al.* [12] find experimental evidence from photoemission microspectroscopy on the core levels of the system $(PbS)_{1.13}TaS_2$ of metal cross substitution of Ta atoms into the PbS layer and Pb atoms into the TaS_2 layer, thus charging the planes and binding them together via Coulomb interaction. They argue that stoichiometry is not a necessary condition for the stabilization of the MLCs. In contrast, in a more recent paper that references the work by Kalänne *et al.*, Kabliman *et al.* [14] use *ab initio* DFT calculations to compare the metal cross substitution mechanism for stoichiometric and nonstoichiometric $(PbS)_{1.14}TaS_2$. The obtained formation energies clearly favor nonstoichiometry and indicate that stoichiometric metal cross substitution cannot stabilize the investigated MLCs. A minimum in the formation energy is reached for an impurity concentration of $n_{\mathrm{Ta_{imp}}} = 0.15$ in the PbS layer. To sustain overall neutrality the substitution of cationic sites within the MX layer by Nb 3^{+} atoms must be balanced by an equal amount of reduced trivalent Nb atoms in the NbS_2 layer. As a result, neighboring layers are electrostatically bound with an interlayer interaction that might be called "cationic coupling" [54]. As a result of this redistribution of charge there is an increase in the electronic population in the NbS_2 layers able to further fill the Nb d_{z^2} band without actually transferring charge from PbS to NbS_2. This could explain the shifts seen in optical reflection spectra and photoelectron spectra without using the concept of charge transfer. Moëlo *et al.* [54] find a substitution of up to 12%, which makes the MLC compound a $(Pb_{0.991}Nb_{0.126}S_{1.136})NbS_2$. This pseudo charge transfer, however, is also unlikely to be responsible for the frequency upshift of the E mode. Our calculations on Pb-NbS_2 and $(PbS)_{1.14}NbS_2$ reproduce the experimentally observed shift and are intrinsically performed on the pure stoichiometric compound. Assuming that the reason is the same in both of the investigated compounds, it can thus be concluded that the reason for the upshift has to be found somewhere else.

(ii) Another mechanism that comes into play as soon as the PbS and the NbS_2 layer are combined and could play a role in stabilizing the MLCs is the coordinative interlayer bonding. The Pb atoms in the PbS layers possess a lone pair of electrons in an orbital that extends in the interlayer van der Waals gap. This enables the Pb atoms to covalently bond to one or two S atoms in the -2 oxidation state of the neighboring NbS_2 layer depending on their relative position along the incommensurate a axis [8]. In fact, it is observed that the Pb atoms in $(PbS)_{1.14}NbS_2$ always protrude into the van der Waals gap [55] in between layers and that interlayer Pb-S distances from Pb atoms in the PbS layer to S atoms in the NbS_2 layer are well within range of normal PbS intralayer bond lengths [56]. Based on the 0.88 nm periodicity observed in Pb-NbS_2 [4], the interlayer Pb-S distance is even shorter than a normal intralayer PbS bond length in the case of the intercalated NbS_2 nanotubes. However, to the best of our knowledge there has been no direct proof of covalent interlayer bonding so far. This idea has only been surfaced in the absence of another mechanism that could explain the stability of misfit layer compounds [10,49] or from theoretical considerations [47]. In addition, it is doubtful that covalent bonds would have a larger influence on the E modes than on the A mode. Instead, one would assume that the out-of-plane movement of sulfur atoms in the latter is more strongly affected than the in-plane movement of the E modes.

(iii) In the context of discussing possible reasons for the upshift of the E modes in intercalated and the MLC compound, it is also interesting to look at other related compounds where frequency shifts occur. In $3R$-NbS_2, for instance, two E modes are seen upshifted considerably compared to $2H$-NbS_2 [39,57]; again the A mode is barely shifted. We have calculated the Raman frequencies of pristine $3R$-NbS_2 and found close to no difference between the Raman frequencies in $2H$- and $3R$-NbS_2. We can thus conclude that the layer stacking order in NbS_2 does not affect the frequency of the phonon modes, contrary to the assumption made in Ref. [36] for explaining the experimentally obtained Raman frequencies in $3R$-NbS_2. Instead, we think that $3R$-NbS_2 is indeed normally nonstoichiometric [40,58] with extra Nb atoms occupying octahedral sites in between the layers. These excess Nb atoms add an additional interlayer force to the weak van der Waals interaction and could be responsible for the observed upshift. As there are only a few of them, the frequency of the in-plane mode highly depends on the local composition and is therefore rather broad. An upshift is seen for Fe_xNbS_2 as well [59] and can be explained along similar lines.

(iv) A yet unexplored way to account for the frequency shift of the in-plane modes in particular combines the charge transfer mechanism with an ionic interlayer coupling. Even in semiconducting intercalant layers like PbS, a non-negligible amount of charge transfer will leave some empty states that enable metallic conduction. Because of the layered nature of the intercalants, this conduction will primarily take place in the a-b plane. In the context of the rigid band model that explains the properties of the MLC as a combination of the properties

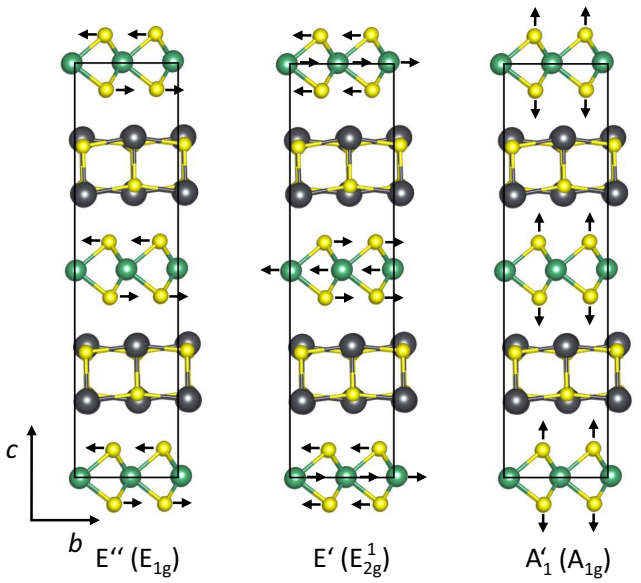

FIG. 6. Atomic displacement patterns of the three main Raman modes in $(PbS)_{1.14}NbS_2$ discussed in the text and listed in Table I. They are derived from the $2H$-NbS_2 E_{1g}, E^1_{2g}, and A_{1g} modes (in brackets) and have E'', E', and A'_1 symmetry, respectively, in the $(PbS)_{1.14}NbS_2$ misfit layer material.

of the two constituents, for the first-order Raman modes of the NbS_2 layer, the atoms in the intercalant layer (here Pb or PbS) do not move (see Fig. 6). With the displacement of atoms in the NbS_2 layer, the charge at the sulfur atoms is moving in-plane for the E modes. As a result, in the neighboring intercalant layer, there will be some in-plane electron charge redistribution. In order to regain minimal energy, this longitudinal charge redistribution will be followed by a restoring force acting on the phonon modes, hence lead to a stiffening of the phonon frequency compared to the parent compound. For the out-of-plane A mode (see Fig. 6), on the other hand, the movement of sulfur atoms will not have the same effect, as charge inside the intercalant layer will not be redistributed significantly along the stacking c direction. The A mode is thus unaffected or even exhibits a slight downshift due to the lack of interlayer interaction with a neighboring NbS_2 layer, much like the redshift seen in few-layer transition metal dichalcogenides compared to the bulk material [60,61]. This charge redistribution model represents a new take on the hitherto unexplained phenomenon of drastic frequency upshifts of Raman modes in intercalated and misfit materials with respect to the respective Raman modes in the transition metal dichalcogenide parent compounds. However, elaborate work is still needed to further support this model and to gain more insight into the reasons for the experimentally observed Raman shifts.

III. CONCLUSION

We have taken Raman measurements of a number of misfit layer $(PbS)_{1.14}NbS_2$ as well as of Pb-NbS_2 nanotubes. Their Raman spectra have in common that they can be interpreted in terms of a superposition of Raman modes of the constituents: First order Raman modes of the transition metal dichalcogenide are found above 250 cm^{-1}, and Raman modes of the intercalant and second order modes of NbS_2 are situated below 200 cm^{-1}. We have calculated the phonon dispersions of the lead intercalated NbS_2 bulk material and the pristine $2H$-NbS_2 as well as the Γ-point phonons of the misfit layer compound to help us attribute the measured Raman modes. Most strikingly, the E^1_{2g}/E' mode of Pb-NbS_2 and $(PbS)_{1.14}NbS_2$, respectively, is shifted up in frequency by more than 30 wave numbers compared to the parent material. The calculations reveal that a similar upshift for the E_{1g}/E'' mode exists. Although this mode is forbidden in the employed backscattering geometry, it can be detected as a peculiarity in the spectra of the Pb-NbS_2 nanotubes. In contrast to the in-plane E type modes, the frequency of the out-of-plane A_{1g}/A'_1 mode in the intercalated and misfit nanotubes stays almost the same as in the parent compound. There are small differences in the magnitude of the measured E^1_{2g}/E' Raman mode upshifts in Pb-NbS_2 and $(PbS)_{1.14}NbS_2$ nanotubes that are used as a starting point for a discussion about the underlying mechanisms for the drastic frequency shifts. We find evidence contradicting the charge transfer model that is brought forward by most of the literature discussing Raman spectra of misfit layer materials in the past. Other interlayer bonding mechanisms such as metal cross substitution and coordinative interlayer bonding are presented and discussed regarding their likelihood of being responsible for the frequency upshifts. We introduce a charge redistribution model that could account for the phenomenon but has yet to be put on solid theoretical ground. Our results will guide future investigations of interlayer interlayer bonding mechanisms in intercalated and misfit layer transition metal dichalcogenides.

ACKNOWLEDGMENTS

We acknowledge financial support of the German-Israeli Foundation (research Grant No. I-1233-302.5/2014) and the European Commission for the Marie S. Curie International Training Network MoWSeS (GA 317451).

[1] R. Tenne and G. Seifert, Annu. Rev. Mater. Res. **39**, 387 (2009).
[2] G. Radovsky, R. Popovitz-Biro, M. Staiger, K. Gartsman, C. Thomsen, T. Lorenz, G. Seifert, and R. Tenne, Angew. Chem. Int. Ed. **50**, 12316 (2011).
[3] G. Radovsky, R. Popovitz-Biro, and R. Tenne, Chem. Mater. **24**, 3004 (2012).
[4] G. Radovsky, R. Popovitz-Biro, D. Stroppa, L. Houben, and R. Tenne, Accts. Chem. Res. **47**, 406 (2014).
[5] J. Rouxel, A. Meerschaut, and G. A. Wiegers, J. Alloys Compd. **229**, 144 (1995).
[6] A. Meerschaut, R. Roesky, A. Lafond, C. Deudon, and J. Rouxel, J. Alloys Compd. **219**, 157 (1995).

[7] G. Wiegers and A. Meerschaut, Mater. Sci. Forum **100-101**, 101 (1992).
[8] G. Wiegers, Prog. Solid St. Chem. **24**, 1 (1996).
[9] J. Brandt, L. Kipp, M. Skibowski, E. E. Krasovskii, W. Schattke, E. Spiecker, C. Dieker, and W. Jäger, Surf. Sci. **532-535**, 705 (2003).
[10] A. R. H. F. Ettema, C. Haas, and T. S. Turner, Phys. Rev. B **47**, 12794 (1993).
[11] A. Meerschaut, Y. Moëlo, L. Cario, A. Lafond, and C. Deudon, Mol. Cryst. Liq. Cryst. Sci. Technol., Sect. A **341**, 1 (2000).
[12] M. Kalläne, K. Rossnagel, M. Marczynski-Bühlow, L. Kipp, H. I. Starnberg, and S. E. Stoltz, Phys. Rev. Lett. **100**, 065502 (2008).
[13] C. Deudon, A. Lafond, O. Leynaud, Y. Moëlo, and A. Meerschaut, J. Solid State Chem. **155**, 1 (2000).
[14] E. Kabliman, P. Blaha, and K. Schwarz, Phys. Rev. B **82**, 125308 (2010).
[15] M. Hangyo, S. Nakashima, Y. Hamada, T. Nishio, and Y. Ohno, Phys. Rev. B **48**, 11291 (1993).
[16] M. Hangyo, K. Kisoda, T. Nishio, S. Nakashima, T. Terashima, and N. Kojima, Phys. Rev. B **50**, 12033 (1994).
[17] K. Kisoda, M. Hangyo, S. Nakashima, K. Suzuki, T. Enoki, and Y. Ohno, J. Phys.: Condens. Matter **7**, 5383 (1995).
[18] K. Kisoda, M. Hangyo, J. Kuroda, H. Harima, and S. Nakashima, Sol. St. Comm. **103**, 597 (1997).
[19] C. Sourisseau, R. Cavagnat, and J. L. Tirado, J. Raman Spectrosc. **23**, 647 (1992).
[20] Q. Lin, C. L. Heideman, N. Nguyen, P. Zschack, C. Chiritescu, D. G. Cahill, and D. C. Johnson, Eur. J. Inorg. Chem. **2008**, 2382 (2008).
[21] P. Jood, M. Ohta, H. Nishiate, A. Yamamoto, O. I. Lebedev, D. Berthebaud, K. Suekuni, and M. Kunii, Chem. Mater. **26**, 2684 (2014).
[22] P. Jood, M. Ohta, O. I. Lebedev, and D. Berthebaud, Chem. Mater. **27**, 7719 (2015).
[23] D. R. Merrill, D. B. Moore, S. R. Bauers, M. Falmbigl, and D. C. Johnson, Materials **8**, 2000 (2015).
[24] D. Reefman, J. Bank, H. B. Brom, and G. A. Wiegers, Solid State Commun. **75**, 47 (1990).
[25] L. Panchakarla, R. Popovitz-Biro, L. Houben, R. Dunin-Borkowski, and R. Tenne, Angew. Chem. Int. Ed. **53**, 6920 (2014).
[26] G. Radovsky, R. Popovitz-Biro, and R. Tenne, Chem. Mater. **26**, 3757 (2014).
[27] G. Radovsky, R. Popovitz-Biro, T. Lorenz, J.-O. Oswig, G. Seifert, L. Houben, R. E. Dunin-Borkowski, and R. Tenne, J. Mater. Chem. C **4**, 89 (2016).
[28] T. Lorenz, J.-O. Oswig, and G. Seifert, Beilstein J. Nanotechnol. **5**, 2171 (2014).
[29] F. Qin, W. Shi, T. Ideue, M. Yoshida, A. Zak, R. Tenne, T. Kikitsu, D. Inoue, D. Hashizume, and Y. Iwasa (unpublished).
[30] O. Madelung, *Semiconductors: Data Handbook*, 3rd ed. (Springer, Berlin, Heidelberg, 2004).
[31] A. Kuc, N. Zibouche, and T. Heine, Phys. Rev. B **83**, 245213 (2011).
[32] D. Bernaerts, S. Amelinckx, G. V. Tendeloo, and J. V. Landuyt, J. Cryst. Growth **172**, 433 (1997).
[33] R. Eppinga and G. Wiegers, Mat. Res. Bull. **12**, 1057 (1977).
[34] G. Radovsky, R. Popovitz-Biro, D. Stroppa, L. Houben, and R. Tenne, Accts. Chem. Res. (2014), see supporting information in Ref. 4.
[35] P. Giannozzi, S. Baroni, N. Bonini, M. Calandra, R. Car *et al.*, J. Phys.: Condens. Matter **21**, 395502 (2009).
[36] S. Nakashima, Y. Tokuda, and A. Mitsuishi, Sol. Stat. Commun. **42**, 601 (1982).
[37] M. Hangyo, K. Kisoda, S. Nakashima, A. Meerschaut, and J. Rouxel, Physica B **219–220**, 481 (1996).
[38] M. Hangyo, T. Nishio, S. Nakashima, Y. Ohno, T. Terashima, and N. Kojima, Jpn. J. Appl. Phys. Suppl. **32**, 581 (1993).
[39] W. McMullan and J. Irwin, Sol. Stat. Commun. **45**, 557 (1983).
[40] M. Fisher and M. Sienko, Inorg. Chem. **19**, 39 (1980).
[41] C. Pereira and W. Liang, J. Phys. C: Solid State Phys. **18**, 6075 (1985).
[42] K. Shirai, K. Kisoda, M. Hangyo, and S. Nakashima, Sol. St. Comm. **103**, 131 (1997).
[43] A. R. H. F. Ettema, S. van Smaalen, C. Haas, and T. S. Turner, Phys. Rev. B **49**, 10585 (1994).
[44] C. Rüscher, C. Haas, S. van Smaalen, and G. Wiegers, J. Phys.: Condens. Matter **6**, 2117 (1994).
[45] Y. Ohno, Phys. Rev. B **48**, 5515 (1993).
[46] C. M. Fang, S. van Smaalen, G. A. Wiegers, C. Haas, and R. A. de Groot, J. Phys.: Condens. Matter **8**, 5367 (1996).
[47] C. M. Fang, A. R. H. F. Ettema, C. Haas, G. A. Wiegers, H. van Leuken, and R. A. de Groot, Phys. Rev. B **52**, 2336 (1995).
[48] Y. Ohno, Phys. Rev. B **44**, 1281 (1991).
[49] A. R. H. F. Ettema and C. Haas, J. Phys.: Condens. Matter **5**, 3817 (1993).
[50] A. R. H. F. Ettema, G. Wiegers, and C. Haas, Surf. Sci. **269–270**, 1161 (1992).
[51] R. Eppinga, G. Wiegers, and C. Haas, Physica B **105**, 174 (1981).
[52] J. Dijkstra, E. A. Broekhuizen, C. F. van Bruggen, C. Haas, R. A. de Groot, and H. P. van der Meulen, Phys. Rev. B **40**, 12111 (1989).
[53] R. Eppinga, G. Sawatzky, C. Haas, and C. van Bruggen, J. Phys. C: Solid State Phys. **9**, 3371 (1976).
[54] Y. Moëlo, A. Meerschaut, J. Rouxel, and C. Auriel, Chem. Mater. **7**, 1759 (1995).
[55] M. Garbrecht, E. Spiecker, K. Tillmann, and W. Jäger, Ultramicroscopy **111**, 245 (2011).
[56] G. Wiegers, A. Meetsma, R. Haange, S. van Smaalen, and J. de Boer, Acta Cryst. **B46**, 324 (1990).
[57] S. Onari and T. Arai, Sol. Stat. Commun. **31**, 577 (1979).
[58] D. Powell and R. Jacobson, J. Solid State Chem. **37**, 140 (1981).
[59] K. Nagao, M. Koyano, S. Katayama, Y. Yamamura, and T. Tsuji, Phys. Stat. Sol. (b) **223**, 281 (2001).
[60] C. Lee, H. Yan, L. E. Brus, T. F. Heinz, J. Hone, and S. Ryu, ACS Nano **4**, 2695 (2010).
[61] M. Staiger, R. Gillen, N. Scheuschner, O. Ochedowski, F. Kampmann, M. Schleberger, C. Thomsen, and J. Maultzsch, Phys. Rev. B **91**, 195419 (2015).